



Geophysical Research Letters

RESEARCH LETTER

10.1029/2020GL090597



Key Points:

- We demonstrate a novel method for using crevasse icequake depths to discriminate between dry and hydrofracture driven surface crevassing
- Icequakes can be used to directly observe and elucidate the crevasse hydrofracture process
- Icequakes show tensile crack failure with opening volumes calculated from moment magnitudes

Supporting Information:

- Supporting Information S1
- Figure S1
- Figure S2

Correspondence to:

T. S. Hudson,
thomas.hudson@earth.ox.ac.uk

Citation:

Hudson, T. S., Brisbourne, A. M., White, R. S., Kendall, J. M., Arthern, R., & Smith, A. M. (2020). Breaking the ice: Identifying hydraulically forced crevassing. *Geophysical Research Letters*, 47, e2020GL090597. <https://doi.org/10.1029/2020GL090597>

Received 1 SEP 2020

Accepted 13 OCT 2020

Accepted article online 19 OCT 2020

Breaking the Ice: Identifying Hydraulically Forced Crevassing

T. S. Hudson¹ , A. M. Brisbourne² , R. S. White³ , J. M. Kendall¹ , R. Arthern² , and A. M. Smith²

¹Department of Earth Sciences, University of Oxford, Oxford, UK, ²British Antarctic Survey, Cambridge, UK, ³Bullard Laboratories, University of Cambridge, Cambridge, UK

Abstract Hydraulically forced crevassing is thought to reduce the stability of ice shelves and ice sheets, affecting structural integrity and providing pathways for surface meltwater to the bed. It can cause ice shelves to collapse and ice sheets to accelerate into the ocean. However, direct observations of the hydraulically forced crevassing process remain elusive. Here we report a novel method and observations that use icequakes to directly observe crevassing and determine the role of hydrofracture. Crevasse icequake depths from seismic observations are compared to a theoretically derived maximum dry crevasse depth. We observe icequakes below this depth, suggesting hydrofracture. Furthermore, icequake source mechanisms provide insight into the fracture process, with predominantly opening cracks observed, which have opening volumes of hundredths of a cubic meter. Our method and findings provide a framework for studying a critical process that is key for the stability of ice shelves and ice sheets and, therefore, future sea level rise projections.

1. Introduction

Hydraulically forced surface crevassing, also referred to as hydrofracture, has the potential to significantly influence the stability of glaciers, ice sheets, and ice shelves (Lai et al., 2020). On glaciers and ice sheets, hydraulically forced crevassing provides a potential pathway for surface meltwater to reach and lubricate the bed (Das et al., 2008; Van Der Veen, 1998; Weertman, 1973), enhancing basal sliding of ice into the ocean (Rignot & Kanagaratnam, 2006), accelerating sea level rise. Hydraulically forced surface crevassing on ice shelves can result in catastrophic failure, with melt ponds promoting fracture that can lead to the collapse of the ice shelf (Hughes, 1983; McGrath et al., 2012; Scambos et al., 2000, 2003). Following ice shelf collapse, land-based glaciers can accelerate into the ocean, since the buttressing provided by the ice shelf no longer exists, again contributing to sea level rise. Understanding the fundamental mechanism of hydraulically forced surface crevassing is therefore a particularly timely topic within glaciology.

Here we present icequake observations from Skeidararjökull, an outlet glacier of the Vatnajökull Ice Cap, Iceland. This glacier is an ideal environment for studying potential hydraulically forced crevassing due to the high levels of surface melt present. Previous studies have used icequakes to infer hydraulically forced crevassing using auxiliary information, such as glacier speed up (Helmstetter et al., 2015), or the presence of meltwater (Carmichael et al., 2012, 2015; Lindner et al., 2020). Others have used seismicity to show that crevassing exhibits tensile faulting (Mikesell et al., 2012; Neave & Savage, 1970; Roux et al., 2010; Walter et al., 2009) and anisotropy (Lindner et al., 2019). We first present a novel method for attributing an icequake to either dry or hydraulically forced crevassing. We then use icequake source mechanisms to confirm the crevassing stress release mechanism. Our results provide for the first time direct evidence of hydrofracture, offering insights into this previously elusive process.

2. Methods

Here we briefly describe the methods for detecting and locating the seismicity, as well as an overview of how the source mechanism inversions are undertaken and moment magnitudes, M_w , are calculated. Two additional methods used in this study are obtaining crevasse icequake depths from P to Rayleigh wave amplitude ratios and the calculation of a theoretical maximum dry crevasse depth, based on the rheology of ice. These methods and theory are too complex to adequately describe in the main text, so we instead describe them in the supporting information (Texts S1 and S2, respectively).

©2020. The Authors.

This is an open access article under the terms of the Creative Commons Attribution-NonCommercial License, which permits use, distribution and reproduction in any medium, provided the original work is properly cited and is not used for commercial purposes.

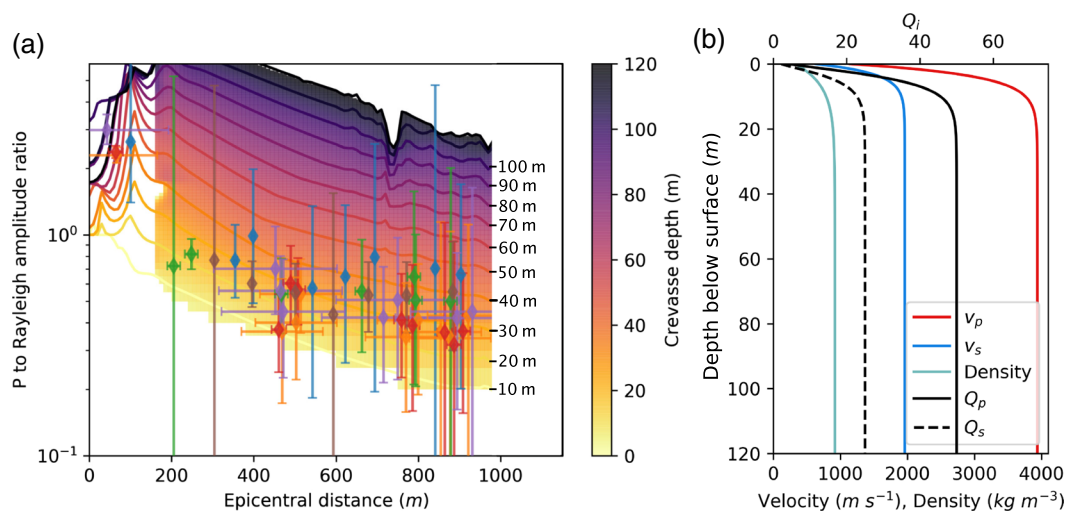


Figure 1. Obtaining depth for crevassing icequakes. (a) Plot of P to Rayleigh wave amplitude ratio with epicentral distance from the source. Observed P to Rayleigh amplitudes for the icequakes presented in Figure 2 are plotted (various colored scatter points). Each point represents observations for an event at one station, and each color signifies all station observations for a single event. P to Rayleigh amplitudes for modeled crevassing icequakes with source depths from 10 to 120 m below surface are indicated by the solid lines, with the 2-D interpolated field plotted at epicentral distances greater than 180 m due to significant radiation pattern effects at lesser distances. (b) The velocity model used for the modeled crevassing icequakes (Gudmundsson, 1989).

The seismicity presented in this study comprises of 1,784 icequakes detected using QuakeMigrate (Hudson et al., 2019; Smith et al., 2020), with the overall catalogue of icequakes described by Hudson et al. (2019). We use automatic P and S wave phase picks to relocate the detected earthquakes using NonLinLoc (Lomax & Virieux, 2000) to obtain more accurate epicentral locations. For the subset of events presented in detail in Figures 1 and 2 (events with focal mechanisms), we manually pick P and S phase arrivals before relocation. The crevassing icequake hypocentral depths for the selected events are poorly constrained by traditional methods and so are instead calculated using P to Rayleigh wave amplitude ratios, with the associated method details given in the supporting information (Text S1).

The icequake source mechanisms are obtained by performing a Bayesian full waveform source inversion using an identical approach to a method detailed by Hudson et al. (2020). Only P wave phases on the vertical component are used since the horizontal components are generally too noisy to use, due to the instruments melting out of the glacier. Theoretically, S and surface waves could also be used to constrain the inversion, but the amplitudes of any S arrivals are generally close to the noise levels and we have low confidence in our ability to model the polarity of dispersive surface waves sufficiently accurately for a moment tensor inversion, given the depth dependent velocity structure of the firn layer at the site. We use a finite difference scheme to model the Green's functions used to produce the synthetic seismograms in the inversion. The depth of the source, a critical parameter affecting the source inversion, is constrained using P to Rayleigh amplitude ratios.

The moment magnitude, M_w , of the icequakes is calculated using a spectral method (Stork et al., 2014) to calculate crack opening volumes. The spectrum of the icequake is calculated by performing multitaper spectral estimation (Krischer, 2016; Prieto et al., 2009) in order to find the long period spectral level and hence the seismic moment release, M_0 . M_w can then be calculated from (Hanks & Kanamori 1979)

$$M_w = \frac{2}{3} \log_{10}(M_0) - 6.0. \quad (1)$$

If one assumes that all the moment release for a given icequake is released via tensile failure, then the opening of a crack, ΔV , can be calculated from (Muller, 2001)

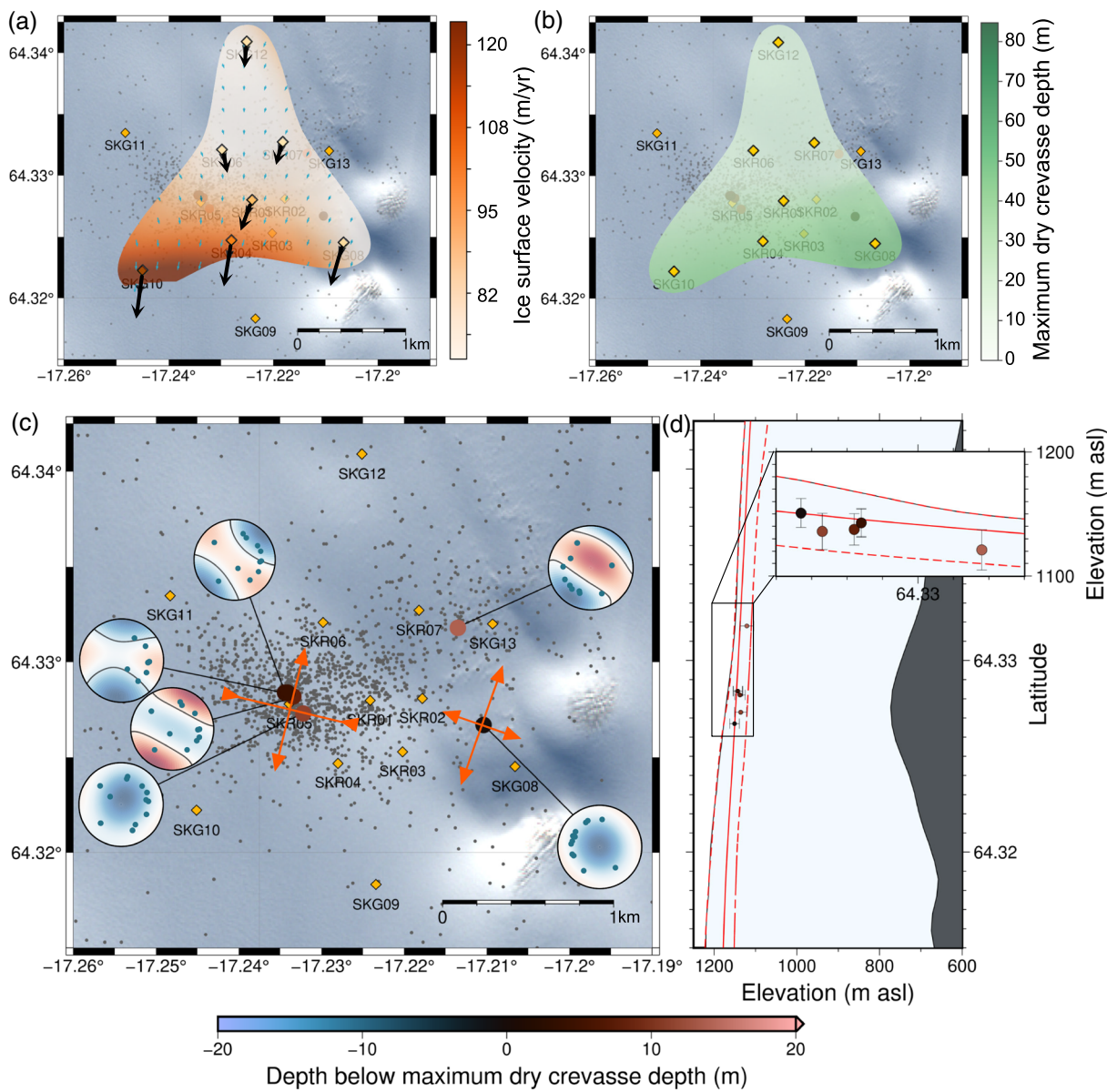


Figure 2. Summary of crevasse icequake observations. (a) The horizontal surface velocity field at the site, derived using GPS data from the highlighted stations. (b) The maximum dry crevasse depth, d^* , calculated using the velocity field in (a). Uncertainty in these fields are given in Figure S2. (c) Map of crevasse icequake locations. Gray scatter points are all the crevasse icequakes detected during the period 19 to 29 June 2014. The icequakes studied in more detail, with derived depths using the P to Rayleigh amplitude method are plotted as larger scatter points, colored by depth below the maximum dry crevasse depth. Upper hemisphere moment tensors for these icequakes are also shown. Principal stress vectors derived from the velocity field in (a) are shown in orange. Seismometer and geophone locations are shown by the yellow diamonds. Satellite image is from the European Space Agency. (d) Plot of the crevassing events in (c) with depth versus latitude projected onto a N-S transect at 17.225°W. The solid and dashed red lines indicate the maximum dry crevasse depth and the associated uncertainty, respectively. The bed topography is derived from ground-penetrating radar (Björnsson, 2017).

$$\Delta V = \frac{M_0}{\lambda + \frac{2}{3}\mu} \quad (2)$$

where λ and μ are the first and second Lamé parameters of the ice, assumed to be approximately 6 and 3 GPa, respectively, here (Podolskiy & Walter, 2016).

3. Results

3.1. Evidence for Dry Fracture Versus Hydrofracture From Crevasse Depth

As a crevasse propagates deeper, the ice fractures, releasing seismic energy as icequakes. Crevasses ordinarily only propagate to a certain depth within the ice column, where the tensile stress field causing crevasse opening is compensated by the ice overburden pressure acting to close the crevasse. We refer to this depth limit as the maximum dry crevasse depth, d^* . However, if the crevasse contains sufficient water, the additional pressure of this water column can overcome the ice overburden pressure and induce hydrofracture, allowing the crevasse to propagate to greater depths (Nick et al., 2010; Van Der Veen, 1998). Therefore, if the observed depth of a crevasse icequake is greater than d^* , then one can infer that the icequake is induced by hydrofracture. This is the fundamental premise of this study.

However, obtaining sufficiently accurate icequake hypocentral depths for comparison to d^* is nontrivial. Seismometer networks are inherently poor at constraining the depth of an earthquake using traditional body wave methods if the source-receiver epicentral distance is much greater than the source depth. This is generally the case in our study. Since the depth of an icequake is critical evidence for or against hydrofracture, a more accurate method is required for constraining hypocentral depth. We use surface wave information in the form of P to Rayleigh wave amplitude ratios to constrain hypocentral depth (Heyburn et al., 2013; Jia et al., 2017; Stein & Wiens, 1986; Tsai & Aki, 1970). Figure 1a shows finite-difference full-waveform modeling results (Larsen et al., 2001) and observations of P to Rayleigh amplitude ratios, plotted against epicentral distance for a range of crevasse depths. The observed amplitude ratios are compared to the model results to calculate the crevassing depths. Independent verification of crevasse depth using P - S delay times from receivers close to the source epicenter is possible for four events (see supporting information Figure S1), giving us confidence that the amplitude ratios provide a sufficiently accurate estimation of icequake depth.

The crevassing depths constrained by the observations in Figure 1 can then be compared to the maximum dry crevasse depths, shown in Figure 2b, derived from the surface velocity field shown in Figure 2a. Figure 2c shows the epicentral locations of the near surface seismicity, with the gray scatter points showing the automatically detected icequakes (Hudson et al., 2019) and the colored scatter points showing a subset of manually relocated events. The majority of this subset of icequakes are located below d^* (solid red line, Figure 2d), on average 7.4 m deeper, from which we infer that they may be induced by hydrofracture.

One potential limitation of using the source depth to discriminate between hydrofracture and dry fracture is that we do not account for dynamic rupture, whereby during the rupture, a crack may propagate deeper than the prevailing stress field otherwise allows, initiated by fracture tip instability (Buehler & Gao, 2006). For the purposes of this study, we treat each icequake as an instantaneous point source, therefore neglecting dynamic rupture. Although this assumption does not fully describe the physics of the source, we deem it appropriate here because of the distinct, high-frequency, and short-duration phase arrivals observed.

Given that the events are predominantly deeper than d^* , we suggest that the majority of these events are likely caused by hydraulically forced crevassing. In any case, the methodologies developed here, which constrain icequake depth from amplitude ratios and use this source depth to discriminate hydrofracture, are important developments for studying hydrofracture-induced crevassing.

3.2. Crevassing Source Mechanisms

Moment tensor inversions constrain whether icequake source mechanisms include explosive, implosive, crack, or shear components. Icequake moments then give the volume of opening, or fault area and displacement, depending upon the icequake source mechanism.

Figure 2c shows the P wave-constrained moment tensor inversion results for the subset of icequakes for which sufficiently accurate depths have been obtained. The inversion results for two of these icequakes are presented in more detail in Figure 3. For both icequakes, the waveform polarities are all correctly inverted for. Lune plots (Tape & Tape, 2012) in Figures 3b and 3d indicate that the most likely source mechanisms for the two icequakes are a closing and an opening crack, respectively, with a negligible shear component in both cases. Regions of compressive and dilatational first arrivals on the focal sphere are to be expected, due to the Poisson effect. Such crack mechanisms are the mode of failure one might expect from either dry or hydraulically forced crevassing. However, after considering the Probability Density Function (PDF) of

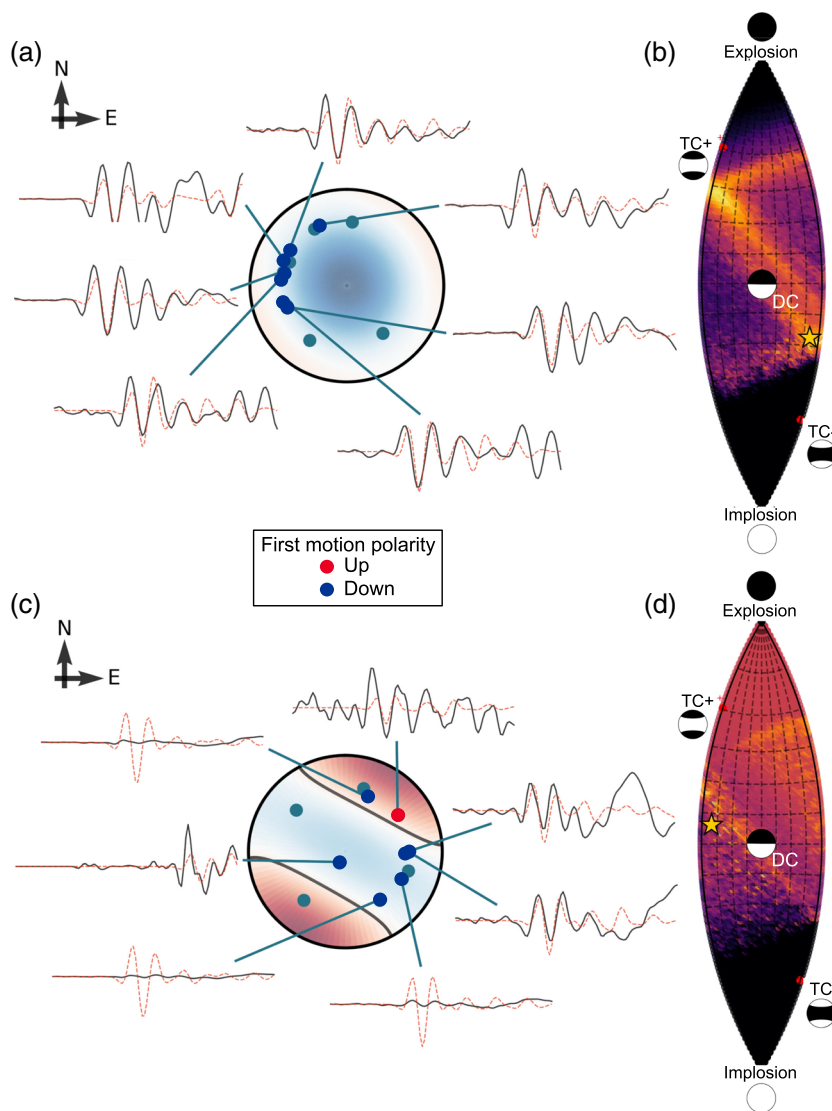


Figure 3. Examples of upper hemisphere crevasse icequake source mechanisms for two of the events in Figure 2. The source mechanisms are constrained only by P wave phases. (a) Source mechanism for a closing-crack crevasse icequake. Black waveforms are observed velocity data through time on the vertical component, red dashed waveforms are the most likely inversion model result. (b) Lune plot (Tape and Tape, 2012) associated with the event in (a), showing the PDF of the full waveform inversion result, indicating the most likely source type. Brighter colors indicate higher binned probability. The gold star indicates the most likely single solution. Black and white source mechanisms show examples of each source type radiation pattern for one possible orientation. (c and d) Same as (a) and (b) except for an opening-crack crevasse icequake.

the inversion solutions for the closing crack icequake in Figure 3b, an opening crack mechanism cannot be eliminated. This ambiguity is due to station geometry on the focal sphere. In any case, an opening or closing crack of a specific orientation is required to represent the observations adequately, as inferred from previous seismic observations (Mikesell et al., 2012; Neave & Savage, 1970; Roux et al., 2010; Walter et al., 2009).

All icequake crack orientations in Figure 2c agree with the principal stress directions calculated from the observed surface velocities, as shown by the orange vectors in Figure 2c, as suggested in previous studies (Garcia et al., 2019; Harper et al., 1998). The apparent closing crack observation for the icequake at 64.327°N , 17.21°W may be supported by the presence of tensile stresses in both principal stress directions. In such a stress regime, a closing crack may be valid, effectively exhibiting two-dimensional necking in the surface-parallel plane.

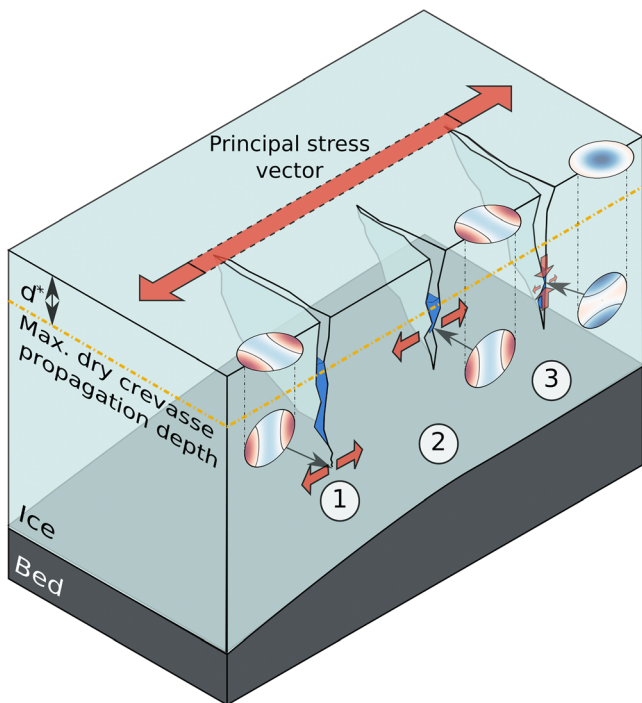


Figure 4. Interpretation of the possible crevasse failure mechanisms observed. (1) A new opening-crack hydrofracture through previously undamaged ice. (2) An opening-crack hydrofracture of a preexisting crack. (3) Closing of a preexisting crack due to the evacuation of water from the crack. Hypothetical source mechanisms are shown for each case.

The moment magnitude of the crevassing icequakes range from -0.4 to -0.9 , calculated using the spectral method of Stork et al. (2014). If we approximate all the failure as tensile, then the volume associated with crack opening or closing ranges from $5.6 \times 10^{-3} \text{ m}^3$ to $2.8 \times 10^{-2} \text{ m}^3$, with an average opening from the six icequakes of $1.6 \pm 0.4 \times 10^{-2} \text{ m}^3$.

We propose several possible mechanisms for generating seismicity below the maximum dry crevasse depth. These interpretations are summarized in Figure 4. The mechanisms are as follows: (1) new cracks opening when the combined deviatoric near-surface stress field and hydrostatic pressure are sufficient to overcome the ice overburden pressure and tensile strength of the ice; (2) preexisting cracks that have closed reopening due to a sufficient head of water in the crevasse; and (3) opened preexisting cracks reclosing as the water is evacuated from the fracture, due to a preferential pressure gradient below the fracture.

For mechanisms 2 and 3, the crevasse must have propagated to that depth via mechanism 1, so mechanism 1 must exist, even if we cannot conclusively observe it here. We observe principal tensile stress amplitudes of greater than 200 kPa (see Figure S2), more than sufficient to overcome an ice yield stress of $\sim 100 \text{ kPa}$ (Paterson, 1994). Mechanism 2 is similar to mechanism 1, except requiring a lower hydrostatic pressure to induce crack opening, and is possible if crevasses have formed upstream and subsequently been closed by principal compressive stresses perpendicular to the crevasse. Such refracturing is proposed in scenarios where there are insufficient volumes of surface meltwater to immediately establish a permanent bed connection (Boon & Sharp, 2003). Mechanism 3 is presented more tentatively, partly due to the potential ambiguity of the closing-crack source mechanism (see Figure 3a), but also because these crevasses would

have to close over sufficiently short time scales to generate the $\sim 100 \text{ Hz}$ source frequencies observed in the P wave spectra. While ice can suddenly fail or reopen a crack over such a short duration, a possible source of driving stresses or pressures required to close cracks this quickly is less conceivable. A crack at greater depth could reopen, evacuating water from above, but envisaging a sufficiently localized stress field is difficult. Alternatively, water may travel through an opening, preexisting crack sufficiently quickly that the crack then immediately closes, although the magnitude of closing would have to dominate over opening to explain a closing-crack observation. In summary, we therefore confidently present mechanisms 1 and 2 but suggest that mechanism 3 is unlikely.

One question that arises is why we do not observe seismicity via mechanisms 1 or 2 occurring all the way to the glacier bed, as is proposed in various studies (Boon & Sharp, 2003; Carmichael et al., 2012; Colgan et al., 2016; Lindner et al., 2020; Van Der Veen, 1998; Weertman, 1973). A reason could be that as such fractures penetrate deeper into the glacier, the energy will be more attenuated, fall below background noise levels, and not be detected. Some icequakes in Hudson et al. (2019) that are located near the bed could be basal crevassing, but there is little evidence to suggest icequakes at intermediate depths. Alternatively, the crevasses at Skeidararjökull might never reach the bed.

These results emphasize the potential information that icequakes hold for elucidating the physics of glacier hydrofracture. Here we only use P waves to constrain the mechanisms, but if one had a more comprehensive dataset with a greater number of receivers and higher SNR, then it may be possible to conclusively rule in or out closing crack source mechanisms. Indeed, although all the mechanisms in Figure 2c show either opening or closing cracks, the variety in orientation and type of crack for these results could be due to (1) poor constraint of the source mechanisms, (2) variation between vertical and sub-vertical crack orientations, and/or (3) actual variations in opening and closing. Furthermore, if one were to invert for a dynamic rupture model of finite length, rather than the instantaneous point source that we assume here, then one might gain additional insight into the physics governing hydrofracture in ice. Another approach to learn more about the hydrofracture process could be to compare observations such as ours to theoretical models of crevasse

vibrational modes to infer crevasse geometry (Lipovsky & Dunham, 2015) or even models of supraglacial lake drainage (Jones et al., 2013).

3.3. Suggestions for Future Deployments

We have a number of suggestions for improving the passive seismic acquisition for future studies of crevassing at glaciers. First, we suggest deploying more densely spaced receivers to improve the constraint of icequake hypocenters and source mechanisms. Ideally, one would deploy instruments spaced at similar distances to the depths of the events being studied, in this case of the order of 10–20 m spacing. Obviously, this would be costly and logistically challenging. However, novel instrumentation such as distributed acoustic sensing (DAS) (Booth et al., 2020; Walter et al., 2020) or seismic nodes would make this feasible. We suggest that one should use a spiral or similar network geometry, so as to have sufficient radial and azimuthal coverage of the study site to constrain source mechanisms. Furthermore, borehole sensors or DAS in a borehole would provide better constraint of hypocentral depths, possibly alleviating the need for the P to Rayleigh amplitude ratio constraint of crevasse depth. In terms of instrumentation deployed, we suggest using geophones rather than broadband seismometers, unless the seismometers are resilient to tilt. To minimize tilt and hence stand the greatest chance of utilizing the horizontal components, we suggest burying the instruments as deep as possible or regularly releveling the instruments. If there is a firn layer present, we also suggest undertaking a simple active seismic refraction survey at the site, in order to constrain the velocity structure. Hopefully, these suggestions will aid others in the design of passive seismic experiments to study crevassing.

4. Implications for Ice Sheet and Ice Shelf Stability

Our findings provide a method for observing hydrofracture at icesheets such as the Greenland Ice Sheet, where although it has been shown that meltwater can drain from the surface to the bed (Das et al., 2008), the mechanism and pathway has not been imaged previously. Calving at the ocean termini of outlet glaciers of the Greenland Ice Sheet could also be enhanced by hydrofracture. Increased calving could be facilitated by precipitation increasing the hydrostatic pressure of water-filled crevasses (O'Neal et al., 2003) or by damage to the upstream ice (Krug et al., 2014), with the depth of this damage through the ice column dependent upon the depth of the crevasses, which we infer here to be controlled by the glacier stress state and hydrofracture. Our method could provide observations of the depth of such damage. The above mechanisms are also hypothesized to be important factors that could accelerate the collapse of the West Antarctic Ice Sheet and cause significant retreat of the East Antarctic Ice Sheet (Pollard et al., 2015).

Some ice shelves exhibit surface melt ponds before undergoing disintegration, whereas others have similar melt ponds but remain intact (Scambos et al., 2000). Crevassing icequakes could provide insight into whether hydrofracture is occurring unnoticed at these apparently stable ice shelves, potentially leading to sudden future catastrophic collapse, or whether hydrofracture is physically suppressed by another mechanism that affects either the stress regime or the fracture toughness of the ice. Ice shelf environments can have relatively high levels of seismic noise compared to some ice sheet settings, due to rifting, calving, and thermal cracking. Our method is likely applicable in such an environment, since Vatnajökull is thought to be similarly noisy due to the high levels of water flow present, as well as seismicity and tremor from nearby volcanoes.

In conclusion, understanding the stability of ice sheets and ice shelves is important for sea level rise projections (Vaughan et al., 2013). Hydrofracture induced crevassing is an important mechanism that at least to some extent, controls the stability of such ice bodies. The methodology and findings we present provide a means of attributing crevassing icequakes to hydrofracture. We show that such icequakes can then be used as an observational basis for studying the physical mechanisms associated with hydrofracture induced crevassing.

Data Availability Statement

Seismic data will be made available on IRIS. Software used includes QuakeMigrate (<https://github.com/QuakeMigrate>); NonLinLoc (<http://alomax.free.fr/nlloc/>); SeisSrcInv (Hudson, 2020a) for the moment tensor inversion; and SeisSrcMoment (Hudson, 2020b) for the moment magnitude calculation.

Acknowledgments

T. H. was funded by a Natural Environment Research Council (NERC) Studentship (NE/L002507/1) for the majority of this work. We thank Antony Butcher for his useful conversations regarding the waveform propagation modeling. We thank Hunter Philson, University of Iceland and the Icelandic Glaciological Society, for his fieldwork support, without which this study would not have been possible. We also thank Finnur Pálsson and the glaciology group at the University of Iceland for the radar bed topography data and Robert Green for preprocessing the data. Seismometers were borrowed from SeisUK (Geophysical Equipment Facility loan number 1022) and NERC British Antarctic Survey.

References

- Björnsson, H. (2017). *The Glaciers of Iceland*. Paris: Atlantis Press. <https://doi.org/10.2991/978-94-6239-207-6>
- Boon, S., & Sharp, M. (2003). The role of hydrologically-driven ice fracture in drainage system evolution on an Arctic glacier. *Geophysical Research Letters*, 30(18), 1916. <https://doi.org/10.1029/2003GL018034>
- Booth, A. D., Christoffersen, P., Schoonman, C., Clarke, A., Hubbard, B., Law, R., et al. (2020). Distributed acoustic sensing (DAS) of seismic properties in a borehole drilled on a fast-flowing Greenlandic outlet glacier. *Geophysical Research Letters*, 47, 13. <https://doi.org/10.1029/2020GL088148>
- Buehler, M. J., & Gao, H. (2006). Dynamical fracture instabilities due to local hyperelasticity at crack tips. *Nature*, 439(7074), 307–310. <https://doi.org/10.1038/nature04408>
- Carmichael, J. D., Joughin, I., Behn, M. D., Das, S., King, M. A., Stevens, L., & Lizarralde, D. (2015). Seismicity on the western Greenland Ice Sheet: Surface fracture in the vicinity of active moulin. *Journal of Geophysical Research: Earth Surface*, 120, 1082–1106. <https://doi.org/10.1002/2014JF003398>.Received
- Carmichael, J. D., Pettit, E. C., Hoffman, M., Fountain, A., & Hallet, B. (2012). Seismic multiple response triggered by melt at Blood Falls, Taylor Glacier, Antarctica. *Journal of Geophysical Research*, 117. <https://doi.org/10.1029/2011JF002221>
- Colgan, W., Rajaram, H., Abdalati, W., Mccutchan, C., Mottram, R., Moussavi, M. S., & Grigsby, S. (2016). Glacier crevasses: Observations, models, and mass balance implications. *Reviews of Geophysics*, 54, 119–161. <https://doi.org/10.1002/2015RG000504>
- Das, S. B., Joughin, I., Behn, M. D., Howat, I. M., King, M. A., Lizarralde, D., & Bhatia, M. P. (2008). Fracture propagation to the base of the Greenland Ice Sheet during supraglacial lake drainage. *Science*, 320(5877), 778–781. <https://doi.org/10.1126/science.1153360>
- Garcia, L., Luttrell, K., Kilb, D., & Walter, F. (2019). Joint geodetic and seismic analysis of surface crevassing near a seasonal glacier-dammed lake at Gornergletscher, Switzerland. *Annals of Glaciology*, 60, 1–13. <https://doi.org/10.1017/aog.2018.32>
- Gudmundsson, M. T. (1989). The Grimsvotn Caldera, Vatnajökull: Subglacial topography and structure of Caldera Infill. *Jokull*, 39, 3–7.
- Hanks, T. C., & Kanamori, H. (1979). A moment magnitude scale. *Journal of Geophysical Research*, 84(B5), 2348. <https://doi.org/10.1029/JB084iB05p02348>
- Harper, J. T., Humphrey, N. F., & Pfeffer, W. T. (1998). Crevasse patterns and the strain-rate tensor: A high-resolution comparison. *Journal of Glaciology*, 44(146), 68–76. <https://doi.org/10.1017/S0022143000002367>
- Helmstetter, A., Nicolas, B., Comon, P., & Gay, M. (2015). Basal icequakes recorded beneath an alpine glacier (Glacier d'Argentière, Mont Blanc, France): Evidence for stick-slip motion? *Journal of Geophysical Research: Earth Surface*, 120, 379–401. <https://doi.org/10.1002/2014JF003288>
- Heyburn, R., Selby, N. D., & Fox, B. (2013). Estimating earthquake source depths by combining surface wave amplitude spectra and teleseismic depth phase observations. *Geophysical Journal International*, 194, 1000–1010. <https://doi.org/10.1093/gji/ggt140>
- Hudson, T. S. (2020a). TomSHudson/SeisSrcInv: Initial release for publication (version v1.0.0-beta). Zenodo. <https://doi.org/10.5281/zenodo.3726697>
- Hudson, T. S. (2020b). TomSHudson/SeisSrcMoment: First formal release (version 1.0.0). Zenodo. <https://doi.org/10.5281/zenodo.4010325>
- Hudson, T. S., Brisbourne, A. M., Walter, F., Graff, D., & White, R. S. (2020). Icequake source mechanisms for studying glacial sliding. *Journal of Geophysical Research: Earth Surface*. <https://doi.org/10.1002/essoar.10502610.1>
- Hudson, T. S., Smith, J., Brisbourne, A., & White, R. (2019). Automated detection of basal icequakes and discrimination from surface crevassing. *Annals of Glaciology*, 60, 1–11.
- Hughes, B. T. (1983). On the disintegration of ice shelves: The role of fracture. *Journal of Glaciology*, 29(101), 98–117. <https://doi.org/10.1017/S0022143000005177>
- Jia, Z., Ni, S., Chu, R., & Zhan, Z. (2017). Joint inversion for earthquake depths using local waveforms and amplitude spectra of Rayleigh waves. *Pure and Applied Geophysics*, 174, 261–277. <https://doi.org/10.1007/s0024-016-1373-1>
- Jones, G. A., Kulessa, B., Doyle, S. H., Dow, C. F., & Hubbard, A. (2013). An automated approach to the location of icequakes using seismic waveform amplitudes. *Annals of Glaciology*, 54, 1–9. <https://doi.org/10.3189/2013AoG64A074>
- Krischer, L. (2016). mtspec Python wrappers 0.3.2. Zenodo. <https://doi.org/10.5281/zenodo.321789>
- Krug, J., Weiss, J., Gagliardini, O., & Durand, G. (2014). Combining damage and fracture mechanics to model calving. *The Cryosphere*, 8, 2101–2117. <https://doi.org/10.5194/tc-8-2101-2014>
- Lai, C., Kingslake, J., Wearing, M. G., Chen, P. C., Gentine, P., Li, H., et al. (2020). Vulnerability of Antarctica's ice shelves to meltwater-driven fracture. *Nature*, 584(7822), 574–578. <https://doi.org/10.1038/s41586-020-2627-8>
- Larsen, S., Wiley, R., Roberts, P., & House, L. (2001). Next-generation numerical modeling: Incorporating elasticity, anisotropy and attenuation. Los Alamos National Laboratory (Vol. LA-UR-01-1).
- Lindner, F., Laske, G., Walter, F., & Doran, A. K. (2019). Crevasse-induced Rayleigh-wave azimuthal anisotropy on Glacier de la Plaine Morte, Switzerland. *Annals of Glaciology*, 60, 96–111. <https://doi.org/10.1017/aog.2018.25>
- Lindner, F., Walter, F., Laske, G., & Gimbert, F. (2020). Glaciohydraulic seismic tremors on an Alpine glacier. *The Cryosphere*, 14(1), 287–308. <https://doi.org/10.5194/tc-14-287-2020>
- Lipovsky, B. P., & Dunham, E. M. (2015). Vibrational modes of hydraulic fractures: Inference of fracture geometry from resonant frequencies and attenuation. *Journal of Geophysical Research: Solid Earth*, 120, 1080–1107. <https://doi.org/10.1002/2014JB011286>
- Lomax, A., & Virieux, J. (2000). Probabilistic earthquake location in 3D and layered models. *Advances in Seismic Event Location, Volume 18 of the Series Modern Approaches in Geophysics*, 101–134. https://doi.org/10.1007/978-94-015-9536-0_5
- McGrath, D., Steffen, K., Scambos, T., Rajaram, H., Casassa, G., Luis, J., & Lagos, R. (2012). Basal crevasses and associated surface crevassing on the Larsen C ice shelf, Antarctica, and their role in ice-shelf instability. *Annals of Glaciology*, 53(60), 10–18. <https://doi.org/10.3189/2012AoG60A005>
- Mikesell, T. D., Van Wijk, K., Haney, M. M., Bradford, J. H., Marshall, H. P., & Harper, J. T. (2012). Monitoring glacier surface seismicity in time and space using Rayleigh waves. *Journal of Geophysical Research*, 117, F02020. <https://doi.org/10.1029/2011JF002259>
- Muller, G. (2001). Volume change of seismic sources from moment tensor. *Bulletin of the Seismological Society of America*, 91(4), 880–884. <https://doi.org/10.1785/0120000261>
- Neave, K. G., & Savage, J. C. (1970). Icequakes on the Athabasca glacier. *Journal of Geophysical Research*, 75(8), 1351–1362. <https://doi.org/10.1029/JB075i008p01351>
- Nick, F. M., Van Der Veen, C. J., Vieli, A., & Benn, D. I. (2010). A physically based calving model applied to marine outlet glaciers and implications for the glacier dynamics. *Journal of Glaciology*, 56(199), 781–794. <https://doi.org/10.3189/002214310794457344>
- O'Neal, S., Echelmeyer, K. A., & Motyka, R. J. (2003). Short-term variations in calving of a tidewater glacier: LeConte Glacier, Alaska, U.S. A. *Journal of Glaciology*, 49(167), 587–598. <https://doi.org/10.3189/172756503781830430>

- Paterson, W. S. B. (1994). *The Physics of Glaciers* (3rd ed.). Oxford: Butterworth-Heinemann.
- Podolskiy, E. A., & Walter, F. (2016). Cryoseismology. *Reviews of Geophysics*, 54, 708–758. <https://doi.org/10.1002/2016RG000526>
- Pollard, D., DeConto, R. M., & Alley, R. B. (2015). Potential Antarctic Ice Sheet retreat driven by hydrofracturing and ice cliff failure. *Earth and Planetary Science Letters*, 412, 112–121. <https://doi.org/10.1016/j.epsl.2014.12.035>
- Prieto, G. A., Parker, R. L., & Vernon, F. L. (2009). A Fortran 90 library for multitaper spectrum analysis. *Computers and Geosciences*, 35(8), 1701–1710. <https://doi.org/10.1016/j.cageo.2008.06.007>
- Rignot, E., & Kanagaratnam, P. (2006). Changes in the velocity structure of the Greenland Ice Sheet. *Science*, 311(5763), 986–990. <https://doi.org/10.1126/science.1121381>
- Roux, P. F., Walter, F., Riesen, P., Sugiyama, S., & Funk, M. (2010). Observation of surface seismic activity changes of an Alpine glacier during a glacier dammed lake outburst. *Journal of Geophysical Research*, 115, 1, F03014–13. <https://doi.org/10.1029/2009JF001535>
- Scambos, T., Hulbe, C., & Fahnestock, M. (2003). Climate-induced ice shelf disintegration in the Antarctic peninsula. *Antarctic Peninsula Climate Variability, Antarctic Research Series*, 79, 79–92.
- Scambos, T. A., Hulbe, C., Fahnestock, M., & Bohlander, J. (2000). The link between climate warming and break-up of ice shelves in the Antarctic Peninsula. *Journal of Glaciology*, 46(154), 516–530. <https://doi.org/10.3189/172756500781833043>
- Smith, J. D., White, R. S., Avouac, J.-P., & Bourne, S. (2020). Probabilistic earthquake locations of induced seismicity in the Groningen region, the Netherlands. *Geophysical Journal International*, 222(1), 507–516. <https://doi.org/10.1093/gji/ggaa179>
- Stein, S., & Wiens, D. A. (1986). Depth determination for shallow teleseismic earthquakes: Methods and results. *Reviews of Geophysics*, 24(4), 806–832. <https://doi.org/10.1029/RG024i004p00806>
- Stork, A. L., Verdon, J. P., & Kendall, J. M. (2014). The robustness of seismic moment and magnitudes estimated using spectral analysis. *Geophysical Prospecting*, 62(4), 862–878. <https://doi.org/10.1111/1365-2478.12134>
- Tape, W., & Tape, C. (2012). A geometric comparison of source-type plots for moment tensors. *Geophysical Journal International*, 190(1), 499–510. <https://doi.org/10.1111/j.1365-246X.2012.05490.x>
- Tsai, Y., & Aki, K. (1970). Precise focal depth determination from amplitude spectra of surface waves. *Journal of Geophysical Research*, 75(29), 5729–5744. <https://doi.org/10.1029/JB075i029p05729>
- Van Der Veen, C. J. (1998). Fracture mechanics approach to penetration of surface crevasses on glaciers. *Cold Regions Science and Technology*, 27(1), 31–47. [https://doi.org/10.1016/S0165-232X\(97\)00022-0](https://doi.org/10.1016/S0165-232X(97)00022-0)
- Vaughan, D., Comiso, J. C., Allison, I., Carrasco, J., Kaser, G., Kwok, R., et al. (2013). Chapter 4: Observations: Cryosphere. In *Climate Change 2013 the Physical Science Basis: Working Group I Contribution to the Fifth Assessment Report of the Intergovernmental Panel on Climate Change* (Chap. 4, pp. 317–382). Cambridge, United Kingdom and New York, NY, USA: Cambridge University Press. <https://doi.org/10.1017/CBO9781107415324.012>
- Walter, F., Gräff, D., Lindner, F., Paitz, P., Köpfli, M., Chmiel, M., & Fichtner, A. (2020). Distributed acoustic sensing of microseismic sources and wave propagation in glaciated terrain. *Nature Communications*, 53(9), 1689–1699. <https://doi.org/10.1038/s41467-020-16442-w>
- Walter, F., Clinton, J. F., Deichmann, N., Dreger, D. S., Minson, S. E., & Funk, M. (2009). Moment tensor inversions of icequakes on Gornergletscher, Switzerland. *Bulletin of the Seismological Society of America*, 99(2A), 852–870. <https://doi.org/10.1785/0120080110>
- Weertman, J. (1973). Can a water-filled crevasse reach the bottom surface of a glacier. *IASH Publ*, 95, 139–145.